MATHEMATICAL MODELING AND COMPUTING, Vol. 13, No. 2, pp. 565–577 (2026)

Haar Wavelet Collocation Method for Stagnation Point Flow over a Nonlinearly Stretching/Shrinking Sheet in Hybrid Carbon Nanotubes with Slip and Suction Effects

Hanani L.[1], Rasedee A. F. N.[2], Koo L. F.[3], Haswaniza N.[1], Hasan M.[4,*]

[1] *Department of Mathematics and Statistics, Faculty of Science, University Putra Malaysia, 43400 Serdang, Selangor, Malaysia*

[2] *Faculty of Economics and Muamalat, University Sains Islam Malaysia, Malaysia*

[3] *Faculty of Humanities, Management and Science, University Putra Malaysia, Bintulu Campus, 97008 Bintulu, Sarawak, Malaysia*

[4] *Centre for Foundation Studies in Science of University Putra Malaysia*

[*] *Corresponding author: mohdhasan@upm.edu.my*

(Received 28 February 2026; Revised 11 June 2026; Accepted 13 June 2026)

This study aims to investigate the stagnation point flow over a nonlinearly stretching/shrinking sheet with the presence of the slip and suction effects in hybrid carbon nanotubes. The mathematical model for the boundary layer flow problem is formulated and solved using numerical techniques based on the Haar Wavelet Collocation method. The single-walled and multi-walled carbon nanotubes were types of hybrid carbon nanotubes used with water as base fluid. The partial differential equations are transformed into nonlinear ordinary differential equations by similarity transformations. Maple software is used to solve these equations. The results were presented in the form of figures including velocity and temperature profiles, local skin friction coefficient and local Nusselt number for different values of hybrid nanoparticles of carbon nanotubes, velocity slip parameter, nonlinear parameter and suction. The outcomes obtained are that the shrinking sheet gives dual solutions at a certain limit, while the stretching sheet gives unique solutions. In addition, the slip effect parameter caused the thinning of the boundary layer thickness and increased the heat transfer rate.

Keywords: *carbon nanotubes; nonlinearly stretching/shrinking; stagnation point; Haar wavelet.*

2020 MSC: 35Q35, 35Q79, 76A02, 76D05 **DOI:** 10.23939/mmc2026.02.565

1. Introduction

Fluid dynamics is a crucial field that studies the behavior of liquids and gases in motion, impacting various disciplines. It involves fundamental equations such as the continuity equation, momentum equation, and energy equation, along with concepts such as Bernoulli's equation and entropy equation. The laws of physics, including conservation of mass, Newton's laws of motion, and thermodynamics, govern fluid motion, enabling the prediction of forces induced by flowing fluids. Understanding fluid dynamics is essential for optimizing processes like mixing, heat transfer, and mass transfer in various industrial and natural systems.

The boundary layer is an important concept in fluid dynamics, particularly in high-speed flows, where it influences drag and flow detachment from solid surfaces. Initially addressed by Ludwig Prandtl, the German physicist and further developed by his students, the boundary layer represents a thin region near a surface where velocity gradients are significant, allowing for the enforcement of the no-slip boundary condition. The von Kármán integral equation and the von Kármán–Pohlhausen

https://orcid.org/0009-0006-1905-1870 (Hanani L.), https://orcid.org/0000-0002-4425-9087 (Rasedee A. F. N.), https://orcid.org/0000-0002-9957-9571 (Koo L. F.), https://orcid.org/0009-0002-4533-7654 (Haswaniza N.), https://orcid.org/0000-0002-7175-6521 (Hasan M.)

method provide mathematical frameworks to analyze boundary layer development, especially in cases like the flow over a flat plate, demonstrating the feasibility of polynomial velocity profiles [1]. The boundary layer concept extends beyond fluid dynamics to multibody systems, where it defines allowable motions within a configuration manifold, emphasizing the dynamics influenced by bilateral constraints and frictional impacts [2].

Heat transfer is the movement of thermal energy by conduction, convection, and radiation between a system and its environment. Heat is transmitted by faster vibrations of particles in solids, and by faster collisions and movements of particles in gases. Conduction mostly takes place in solids, where temperature gradient and thermal conductivity of the material determine how quickly heat moves through it. Convection is the predominant method of heat transfer in liquids and gases. It involves the movement of fluids and is essential for cooling systems in electrical equipment. When solid surfaces are separated by air gaps, radiation heat transfer, which takes the form of electromagnetic radiation, is important. Designing effective heat exchangers and other thermal equipment for use in a variety of industries, including chemical plants, gas processing, and refining, requires a thorough understanding of these heat transfer mechanisms.

The Prandtl number (Pr) is a dimensionless parameter utilized in fluid mechanics and heat transfer studies to quantify the ratio of momentum diffusivity to thermal diffusivity in a fluid medium. It was proposed by Ludwig Prandtl in 1904, a pioneering figure in fluid dynamics and aerodynamics. It serves to assess how heat transfer compares to momentum transfer within the fluid. Mathematically, the Prandtl number is defined as the ratio of kinematic viscosity to thermal diffusivity of the fluid. The Prandtl number is crucial in analyzing convection and boundary layer flows where both heat and momentum transfer mechanisms are significant. It provides insights into the relative efficiencies of these processes within various fluid systems, guiding the understanding and prediction of heat transfer rates in practical applications.

NEC Corporation, and IBM Research had patents on CNTs in 1993 (Ref. [3] at NEC; Ref. [4] at IBM). Carbon Nanotubes (CNTs) are nanomaterials consisting of carbon with a diameter in the nanometer scale. They are an allotrope of carbon and have been extensively studied due to their unique properties. These properties include SWCNTs can be metallic with a high current carrying capacity or semiconducting based on their structure like metallic where it has highest electrical conductance and moderate bandgap-semiconducting. In addition, carbon nanotubes exhibit high thermal conductivity, enabling them to be used for thermal management, extremely strong with a Young's modulus around 1 terapascal, and extremely stiff making them ten times as strong as steel. Chemically, carbon nanotubes are resistant to corrosion and neutral. There are two types of carbon nanotubes, this depends on their structure: Single-walled (SWCNTs) and Multi-walled (MWCNTs). With diameters ranging from 0.5 to 2.0 nanometers, SWCNTs can be viewed as cutouts from a two-dimensional graphene sheet rolled up to construct the hollow cylinder while MWCNTs contain nested SWCNTs in a tube-in-tube configuration with diameters ranging from 1 to 100 nanometers. Based on Navrotskaya et al. [5], CNTs materials have been acknowledged as suitable materials for environmental applications, resulting in a significant increase in the production of HNFs from these materials in the field of nanotechnology. The growing utilization of CNTs in HNFs is further backed by various studies highlighting their excellent physical and thermal properties. Nevertheless, there is a lack of discourse on the experimental and theoretical examination of hybrid-based carbon nanotubes, particularly in the context of suspending single and multi-walled carbon nanotubes (SWCNTs and MWCNTs) as potential HNFs. Several studies by Al-Hanaya et al. [6], Aladdin and Bachok [7], Kumar and Sulochana [8], and Tabassum et al. [9] have been identified in the literature for actively investigating the manipulation of hybrid SWCNTs and MWCNTs to analyze flow and heat transfer behavior across different geometrical surfaces. Their findings collectively suggest that hybrid SWCNTs and MWCNTs performed better than single nanofluids, whether SWCNTs or MWCNTs.

Stagnation point flow refers to the phenomenon where a fluid, approaching an object, comes to a complete stop at a specific point on the object's surface. This stagnation point is characterized by the fluid velocity relative to the object dropping to zero, resulting from the conversion of kinetic energy into pressure energy as the fluid is forced to decelerate. Depending on the object's shape and the flow conditions, stagnation points can occur either on the front or behind the object. The stretching surface is one that is extended in its own plane, which occurs when the boundary velocity shifts away from a fixed point. Plastic and rubber sheet aerodynamic extrusion, hot rolling, wire drawing, and glass-fiber creation are some instances of this flow in industrial operations and engineering. While the shrinking surface is one that has shrunk when the boundary velocity approaches a fixed point. Some popular applications for shrinking surfaces include shrinking film for bulk product packaging and capillary effects in microscopic pores. Norzawary and Bachok [10] examined slip flow in carbon nanotubes (CNTs) with suction/injection via nonlinearly stretching/shrinking sheets where water serves as the base fluid alongside single-walled and multi-walled CNTs and both velocity slip and thermal slip were included in this investigation.

In recent years, the wavelet approach has been widely used in the numerical approximations area. Numerous types of wavelets such as Haar-wavelet, Legendre wavelet and Mathieu wavelet have been applied in numerical solutions for instance partial differential equations (PDEs), ordinary differential equations (ODEs) and integral equations. In 1910, the Haar-wavelet was discovered by Hungarian mathematician known as Alfred Haar. It is prominent among other researchers due to its functional properties as it is simple orthogonality and applicability. The Haar wavelets are the simplest among other wavelets and consist of piecewise constant functions. The Haar-Wavelet Collocation Method (HWCM) has been extensively studied in various research papers. For example, Ahsan et al. [11] introduced the Haar-wavelet collocation method for solving Riccati equations with different boundary conditions, showcasing stability and convergence. Additionally, Ahsan et al. [12] applied the HWCM to linear and nonlinear inverse problems with unknown heat sources, transforming ill-posed problems into well-conditioned algebraic equations without regularization, demonstrating efficiency and accuracy.

2. Haar Wavelets

Haar wavelets are the mathematically simplest orthonormal wavelet with a compact support, dyadic, discrete, formed from pairs of piecewise constant functions. The conceptual simplicity of the Haar-wavelet method has made it helpful for solving integral and differential equations. Based on Šarler et al. [13], Haar wavelets for $0 \leqslant x < 1$ are defined as

$$h_i(x) = \begin{cases} 1, & \text{for} \quad \alpha \leqslant x < \beta, \\ -1, & \text{for} \quad \beta \leqslant x < \gamma, \\ 0, & \text{otherwise,} \end{cases} \tag{1}$$

where $\alpha = \frac{k}{m}$, $\beta = \frac{k+\frac{1}{2}}{m}$, $\gamma = \frac{k+1}{m}$.

Based on the definition given, the integer $m = 2^j$ where $j = 0, 1, \ldots, J$ indicates the wavelet level, where J is the maximal of resolution, and the integer $k = 0, 1, \ldots, m-1$ is the translation parameter. The formula $i = m + k + 1$ is used to calculate the index i in Eq. (1) with the minimal values $m = 1$, $k = 0$, then $i = 2$. So, the maximal value of i is $i = 2M = 2^{J+1}$. The collocation points are considered as below:

$$x_j = \frac{j - \frac{1}{2}}{2M}, \quad j = 1, 2, \ldots, 2M.$$

The one-dimensional Haar wavelet family for $x \in [0, 1)$ can be defined as the Haar wavelet associated with the mother wavelet.

$$h_i(x) = \begin{cases} 1, & \text{for} \quad 0 \leqslant x < \frac{1}{2}, \\ -1, & \text{for} \quad \frac{1}{2} \leqslant x < 1, \\ 0, & \text{otherwise.} \end{cases}$$

For case $i = 1$, it is known as scaling function

$$h_1(x) = \begin{cases} 1, & \text{for} \quad 0 \leqslant x < 1, \\ 0, & \text{otherwise.} \end{cases}$$

Based on Lepik [14], the notations for Haar function and their integrals are as follows:

$$p_{i,1}(x)=\int_0^x h_i(x')\,dx',\quad p_{i,a+1}(x)=\int_0^x p_{i,a}(x')\,dx',\quad a=1,2,\ldots.$$

By using Eq. (1), sets of integrals can be evaluated and extended and the first three of them are given as follows:

$$p_{i,1}(x)=\begin{cases} x-\alpha, & \text{for } \alpha\leqslant x<\beta,\\ \gamma-x, & \text{for } \beta\leqslant x<\gamma,\\ 0, & \text{otherwise.}\end{cases}$$

$$p_{i,2}(x)=\begin{cases} \frac{1}{2}(x-\alpha)^2, & \text{for } \alpha\leqslant x<\beta,\\ \frac{1}{4m^2}-\frac{1}{2}(\gamma-x)^2, & \text{for } \beta\leqslant x<\gamma,\\ \frac{1}{4m^2} & \text{for } \gamma\leqslant x<1,\\ 0, & \text{otherwise,}\end{cases}\qquad p_{i,3}(x)=\begin{cases} \frac{1}{6}(x-\alpha)^3, & \text{for } \alpha\leqslant x<\beta,\\ \frac{1}{4m^2}(x-\beta)-\frac{1}{6}(\gamma-x)^3, & \text{for } \beta\leqslant x<\gamma,\\ \frac{1}{4m^2}(x-\beta), & \text{for } \gamma\leqslant x<1,\\ 0, & \text{otherwise.}\end{cases}$$

The following notation was also introduced

$$C_{i,1}(x)=\int_0^L P_{i,1}(x')\,dx',\quad C_{i,2}(x)=\int_0^L h_i(x')\,dx'.$$

Any square integrable function $f(x)$ in the interval $0\leqslant x<1$ can be expressed as an infinite sum of Haar wavelets as

$$f(x)=\sum_{i=1}^{\infty}a_ih_i(x),$$

where a_i, $i=1,2,\ldots$ are the Haar coefficients.

3. Mathematical Formulation

A steady boundary layer of hybrid carbon nanotubes for the stagnation point flow over a nonlinearly stretching/shrinking sheet with slip and suction effects by Haar wavelet was studied numerically. Figure 1 shows the schematic illustration of the boundary layer problem where the x-axis is considered along the shrinking sheet in the vertical direction while the y-axis is perpendicular to it. Then, the sheet expands and contracts with the velocity of the free stream $U_w(x)=ax^n$ and the velocity of the stretching/shrinking sheet $U_\infty(x)=bx^n$, where a, b, and n are positive constants such that a, $b>0$, and $n>1$. The presence of slip effect condition $u=U_w(x)+L(\frac{\partial u}{\partial y})$, given that $L=L_1x^{-(\frac{n-1}{2})}$ and $M=M_1x^{-(\frac{n-1}{2})}$ are the slip factor and the presence of suction effect condition $v=V(x)$, given that $V(x)$ is the mass transfer velocity. The surface is maintained at constant surface temperature T_w and constant temperature ambient hybrid CNT nanofluids T_∞.

As a consequence of the previously mentioned boundary layer assumptions, the equations of continuity, momentum, and energy are formulated by Samat et al. [15],

$$\frac{\partial u}{\partial x}+\frac{\partial v}{\partial y}=0, \tag{2}$$

$$u\frac{\partial u}{\partial x}+v\frac{\partial u}{\partial y}=U_\infty\frac{dU_\infty}{dx}+\frac{\mu_{hnf}}{\rho_{hnf}}\frac{\partial^2 u}{\partial y^2}, \tag{3}$$

$$u\frac{\partial T}{\partial x}+v\frac{\partial T}{\partial y}=\alpha_{hnf}\frac{\partial^2 T}{\partial y^2} \tag{4}$$

along with the boundary conditions,

$$u=U_w(x)+L\frac{\partial u}{\partial y},\quad v=V(x),\quad T=T_w+M\frac{\partial T}{\partial y}\ \text{ at }\ y=0,$$
$$u\to U_\infty,\quad T\to T_\infty\ \text{ as }\ y\to\infty. \tag{5}$$

Then, the correlation of the physical properties is shown in Table 1 [15].

Given that φ_1 and φ_2 are hybrid nanoparticle volume fraction SWCNT and hybrid nanoparticle volume fraction MWCNT respectively, (ρC_p) and k is the heat capacity and thermal conductivity which given that the subscript f, nf, hnf, $SWCNT$, and $MWCNT$ represent 'fluid', 'nanofluid', 'hybrid nanofluid', 'Single-walled carbon nanotubes' and 'Multi-walled carbon nanotubes', respectively.

Table 1. Hybrid Carbon Nanotubes thermophysical properties.

Properties	Hybrid Carbon Nanotubes Correlations
Dynamic Viscosity	$\mu_{hnf} = \frac{\mu_f}{(1-\varphi_1)^{2.5}(1-\varphi_2)^{2.5}}$
Hybrid CNTs Density	$\rho_{hnf} = (1-\varphi_2)[(1-\varphi_1)\rho_f + \varphi_1\rho_{SWCNT}] + \varphi_2\rho_{MWCNT}$
Thermal Diffusivity	$\alpha_{hnf} = \frac{k_{hnf}}{(\rho C_p)_{hnf}}$
Heat Capacity	$(\rho C_p)_{hnf} = (1-\varphi_2)[(1-\varphi_1)(\rho C_p)_f + \varphi_1(\rho C_p)_{SWCNT}] + \varphi_2(\rho C_p)_{MWCNT}$
Thermal Conductivity	$k_{hnf} = \left(\frac{(1-\varphi_2)+2\varphi_2(\frac{k_{MWCNT}}{k_{MWCNT}-k_{nf}})\ln\frac{k_{MWCNT}+k_{nf}}{k_{nf}}}{(1-\varphi_2)+2\varphi_2(\frac{k_{nf}}{k_{MWCNT}-k_{nf}})\ln\frac{k_{MWCNT}+k_{nf}}{k_{nf}}}\right)k_{nf}$, where $k_{nf} = \left(\frac{(1-\varphi_1)+2\varphi_1(\frac{k_{SWCNT}}{k_{SWCNT}-k_f})\ln\frac{k_{SWCNT}+k_f}{k_f}}{(1-\varphi_1)+2\varphi_1(\frac{k_f}{k_{SWCNT}-k_f})\ln\frac{k_{SWCNT}+k_f}{k_f}}\right)k_f$

Then, Samat et al. [15] proved that transforming PDEs into ODEs can make it less complex to examine the physical system of fluid flow and heat transfer by similarity variables and also stated that ODEs are more numerically stable than PDEs based on previous researchers. These similarity variables can be applied in the following expressions:

$$\eta = \left(\frac{b(n+1)}{2\nu_f}\right)^{\frac{1}{2}} y\, x^{\frac{n-1}{2}}, \quad \psi = \left(\frac{2b\nu_f}{n+1}\right)^{\frac{1}{2}} x^{\frac{n+1}{2}} f(\eta), \quad T = T_\infty + (T_w - T_\infty)\theta(\eta), \tag{6}$$

as η is the variable of similarity and ψ is the function of a stream. Next, the velocity components can be represented as $u = \frac{\partial\psi}{\partial y}$, $v = -\frac{\partial\psi}{\partial x}$. By utilizing the defining parameter, Eq. (2) is satisfied and the remaining Eqs. (3)–(4) are reduced as follows:

$$A_1 f'''(\eta) + f(\eta)f''(\eta) + A_2\left(1 - f'(\eta)^2\right) = 0, \tag{7}$$

$$\frac{1}{\mathrm{Pr}} A_3\theta''(\eta) + f(\eta)\theta'(\eta) = 0, \tag{8}$$

where $A_1 = \frac{\mu_{hnf}/\mu_f}{\rho_{hnf}/\rho_f}$, $A_2 = \frac{2n}{n+1}$, n is the nonlinear parameter, and $A_3 = \frac{k_{hnf}/k_f}{(\rho C_p)_{hnf}/(\rho C_p)_f}$.

Along with the transformed boundary conditions,

$$\begin{gathered} f'(0) = \varepsilon + \sigma f''(0), \quad f(0) = S, \quad \theta(0) = 1 + \sigma_t\theta'(0), \\ f'(\eta) \to 1, \quad \theta(\eta) \to 0 \ \text{ as } \ \eta \to \infty \end{gathered} \tag{9}$$

where $\varepsilon = \frac{a}{b}$ is the stretching/shrinking velocity parameter in dimensionless units. σ is the velocity slip parameter, σ_t is the thermal slip parameter, and $S > 0$ is the suction. In addition, Prandtl number is presented by $\mathrm{Pr} = \frac{v}{\alpha}$. Then, the physical quantities required are local skin friction coefficient, C_f and local Nusselt number, Nu_x,

$$C_f = \frac{\mu_{hnf}}{\rho_f U_\infty^2}\left(\frac{\partial u}{\partial y}\right)_{y=0}, \tag{10}$$

$$\mathrm{Nu}_x = \frac{-x\, k_{hnf}}{k_f(T_w - T_\infty)}\left(\frac{\partial T}{\partial y}\right)_{y=0}. \tag{11}$$

Hence, the above physical quantities are

$$C_f(\mathrm{Re}_x)^{1/2} = \frac{\mu_{hnf}}{\mu_f}\sqrt{\frac{n+1}{2}} f''(0), \tag{12}$$

$$\mathrm{Nu}_x(\mathrm{Re}_x)^{-1/2} = -\frac{k_{hnf}}{k_f}\sqrt{\frac{n+1}{2}}\theta'(0), \tag{13}$$

and $\mathrm{Re}_x = \frac{U_\infty x}{v_f}$ is the local Reynold number.

Numerical solution by Haar wavelet collocation method (HWCM). The semi-infinite physical domain $[0,\infty)$ should be transformed to an appropriate Haar wavelet context, which can be confined to $[0,1]$. The coordinate transformation, $\xi=\frac{\eta}{\eta_\infty}$ transformed the variable to $F(\xi)=\frac{f(\eta)}{\eta_\infty}$ and $\theta_1(\xi)=\frac{\theta(\eta)}{\eta_\infty}$, ensuring that the boundary conditions are met. Then, Eqs. (7) and (8) can be transformed to

$$A_1F'''(\xi)+\eta_\infty^2F(\xi)F''(\xi)+A_2\eta_\infty^2(1-F'(\xi)^2)=0, \tag{14}$$

$$\frac{1}{\Pr}A_3\theta_1''(\xi)+\eta_\infty^2F(\xi)\theta_1'(\xi)=0, \tag{15}$$

where $A_1=\frac{\mu_{hnf}/\mu_f}{\rho_{hnf}/\rho_f}$, $A_2=\left(\frac{2n}{n+1}\right)$, and $A_3=\frac{k_{hnf}/k_f}{(\rho C_p)_{hnf}/(\rho C_p)_f}$.

The boundary conditions of (9) are transformed to

$$F'(0)=\varepsilon+\frac{\sigma F''(0)}{\eta_\infty},\quad F(0)=\frac{S}{\eta_\infty},\quad \theta_1(0)=\frac{1+\sigma_t\theta_1'(0)}{\eta_\infty},$$
$$F'(\xi)\to 1,\quad \theta_1(\xi)\to 0,\quad \text{as}\quad \xi\to\infty. \tag{16}$$

The higher order of derivatives for (14) and (15) are approximated by Haar wavelet,

$$F'''(\xi)=\sum_{i=1}^{2^{J+1}}a_ih_i(\xi), \tag{17}$$

$$\theta_1''(\xi)=\sum_{i=1}^{2^{J+1}}d_ih_i(\xi). \tag{18}$$

Letting $A=\frac{\sigma}{\eta_\infty}+1$ and $D=-\frac{\sigma_t}{\eta_\infty}-1$. Then, the corresponding lower order of derivatives are integrated using (17) and (18) can be interpreted as

$$F''(\xi)=\sum_{i=1}^{2^{J+1}}a_i\left(P_{i,1}(\xi)-\frac{C_i}{A}\right)+\frac{1}{A}(1-\varepsilon), \tag{19}$$

$$F'(\xi)=\sum_{i=1}^{2^{J+1}}a_i\left[P_{i,2}(\xi)-\frac{C_i}{A}\left(\xi+\frac{\sigma}{\eta_\infty}\right)\right]+\frac{1}{A}(1-\varepsilon)\left(\xi+\frac{\sigma}{\eta_\infty}\right)+\varepsilon, \tag{20}$$

$$F(\xi)=\sum_{i=1}^{2^{J+1}}a_i\left[P_{i,3}(\xi)-\frac{C_i}{A}\left(\frac{\xi^2}{2}+\frac{\sigma\xi}{\eta_\infty}\right)\right]+\frac{1}{A}(1-\varepsilon)\left(\frac{\xi^2}{2}+\frac{\sigma\xi}{\eta_\infty}\right)+\varepsilon\xi+\frac{S}{\eta_\infty}, \tag{21}$$

$$\theta_1'(\xi)=\sum_{i=1}^{2^{J+1}}d_i\left(P_{i,1}(\xi)+\frac{C_i}{D}\right)+\frac{1}{D\eta_\infty}, \tag{22}$$

$$\theta_1(\xi)=\sum_{i=1}^{2^{J+1}}d_i\left(P_{i,2}(\xi)+\frac{C_i\xi}{D}+\frac{C_i\sigma_t}{D\eta_\infty}\right)+\frac{1}{\eta_\infty}\left(\frac{\xi}{D}+\frac{\sigma_t}{D\eta_\infty}+1\right). \tag{23}$$

Then, Eqs. (19)–(23) are used in (14) and (15), and by applying the collocation point

$$\xi_j=\frac{j-\frac{1}{2}}{2^{J+1}},\quad j=1,2,\dots,2^{J+1}, \tag{24}$$

a numerical solution for the system of nonlinear equations with 2^{J+1} unknown wavelet coefficients can be derived.

4. Results and Discussion

The analytical solutions for the ODEs Eqs. (7) and (8) along with boundary condition equations (9) have been solved and the numerical solutions can be achieved using Maple software (Maple 2015.0) for different values of hybrid nanoparticle volume fractions MWCNT φ_2, nonlinear parameter n, velocity slip parameter σ and suction parameter S. Consider the values of hybrid nanoparticle volume fraction MWCNT φ_2 in the range from 0 to 0.2 and Pr = 6.2 for base fluid which is water. Meanwhile, for value nonlinear parameter n is 1, 2, and 3. Then, for velocity slip parameter σ is taken from Norzawary and Bachok [10] where the value is in the range from 0 to 0.4. Meanwhile, for the values of suction parameter S are -0.1, 0, and 0.1. The basic properties of hybrid CNTs and base fluid are shown in Table 2 [15]. The present results of $f''(0)$ and $-\theta'(0)$ have been validated with past studies result by Samat et al. [15] as in Table 3.

Table 2. Thermophysical properties of hybrid CNTs.

Properties	SWCNTs	MWCNTs	Base fluid (water)
Density, ρ ($\mathrm{kg\,m^{-3}}$)	2600	1600	997.1
Heat Capacity, C_p ($\mathrm{J\,kg^{-1}K^{-1}}$)	425	796	4179
Thermal Conductivity, k ($\mathrm{W\,m^{-1}K^{-1}}$)	6600	3000	0.613

Table 3. Comparison between the current model and Samat et al. model, $n = 1$.

Samat et al.		Current result	
$f''(0)$	$-\theta'(0)$	$f''(0)$	$-\theta'(0)$
1.1867	0.1828	1.1874	0.1907

Figures 1 and 2 show the impact of MWCNT nanoparticle φ_2 on the velocity profile $f'(\eta)$ and temperature profile $\theta(\eta)$ for shrinking case ($\varepsilon < -1$) along with the SWCNT nanoparticle φ_1 fixed to 0.1, $\sigma_1 = \sigma_2 = 0.2$, $n = 2$, $\varepsilon = -1.2$, and $S = 0.1$. It is found that $f'(\eta)$ escalates within the momentum boundary layer due to the increasing value of φ_2 for the first and second solutions. Meanwhile, $\theta(\eta)$ reduces with the increasing value of φ_2 for both solutions. Consequently, it causes the thinning of the boundary layer thickness. Thus, duality exists for $\varepsilon = -1.2$. Figures 3 and 4 present the results of the skin friction coefficient $f''(0)$ and the heat transfer of the surface $-\theta'(0)$ for certain values of the stretching/shrinking parameter ε for diverse values of the hybrid nanoparticle volume fraction MWCNT φ_2 with $\varphi_1 = 0.1$, $\sigma_1 = \sigma_2 = 0.2$, $n = 2$ and $S = 0.1$. It is noticed that duality exists when $\varepsilon \leqslant -1$ and also unique solutions were obtained when $\varepsilon > -1$, but there is no solution when $\varepsilon < \varepsilon_c$ due to the boundary layer separations are bound to occur and the boundary layer approximation cannot be done further this critical values ε_c. Moreover, the significance of $f''(0)$ are raised with the increasing values of φ_2. Whereas, the increasing values of φ_2 caused the reduction values of $-\theta'(0)$ when $\varepsilon > -1$ and the inverse pattern are discovered when $\varepsilon < -1$. Hence, by lowering the momentum boundary layer thickness cause the increasing of skin frictions and heat transfer at the surface.

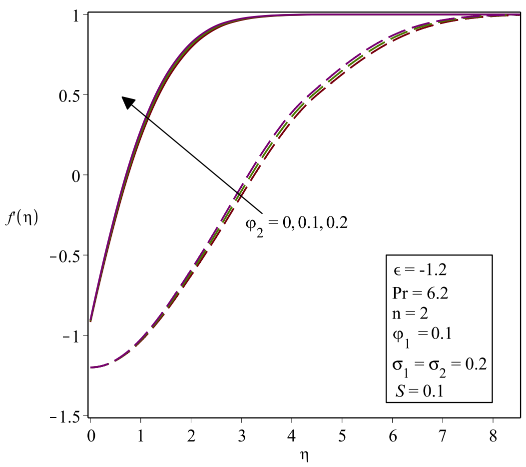

Figure 1. Velocity profile with σ_1, σ_2 and S for different φ_2.

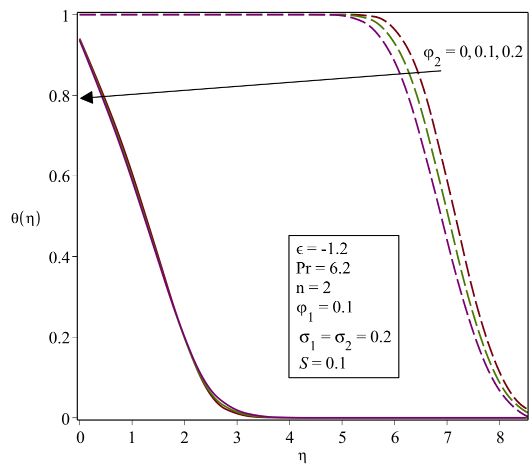

Figure 2. Temperature profile with σ_1, σ_2 and S for different φ_2.

Figures 5 and 6 display the effect of various velocity slip σ_1 values on the velocity profile $f'(\eta)$ and temperature profile $\theta(\eta)$ for shrinking case ($\varepsilon < -1$) with $\varphi_1 = \varphi_2 = 0.1$, $\sigma_2 = 0.2$, $n = 2$, $\varepsilon = -1.2$, and $S = 0.1$. From both figures, $f'(\eta)$ increases in the momentum boundary layer for first solution but decreases for second solution. Moreover, the result for $\theta(\eta)$ shows that it decreases in thermal boundary layer for both first solution and second solution. Figures 7 and 8 show the graphs $f''(0)$

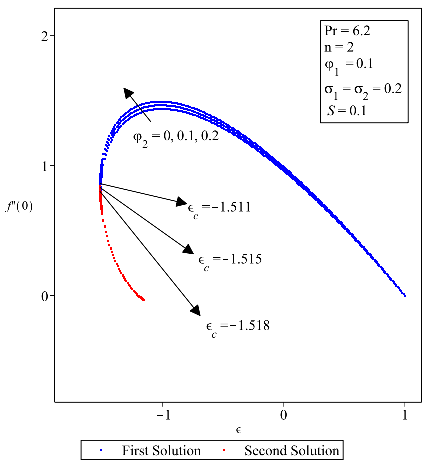

Figure 3. $f''(0)$ with ε, σ_1, σ_2 and S for different φ_2.

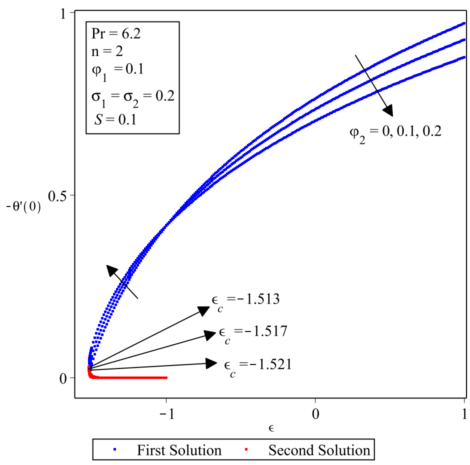

Figure 4. $-\theta(0)$ with ε, σ_1, σ_2 and S for different φ_2.

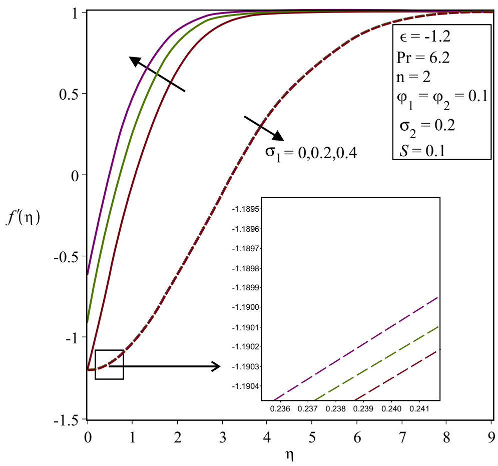

Figure 5. Velocity profile with σ_2 and S for different σ_1.

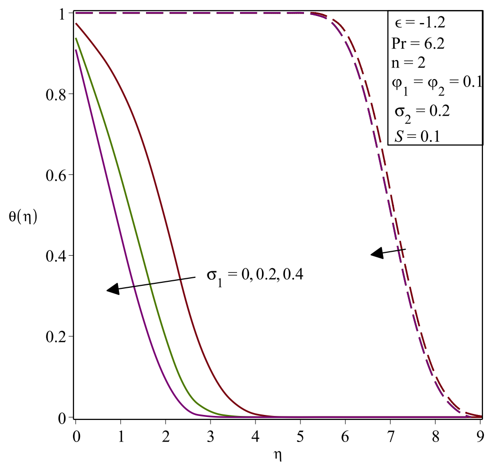

Figure 6. Temperature profile with σ_2 and S for different σ_1.

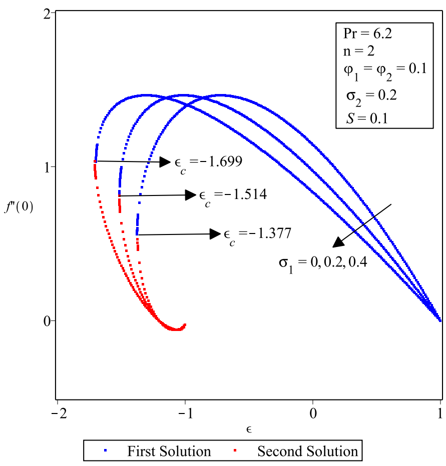

Figure 7. $f''(0)$ with ε, σ_2 and S for different σ_1.

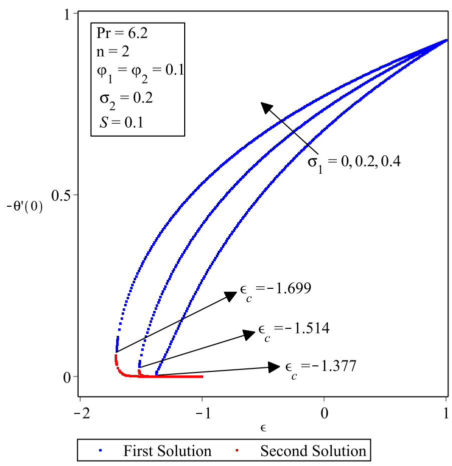

Figure 8. $-\theta'(0)$ with ε, σ_2 and S for different σ_1.

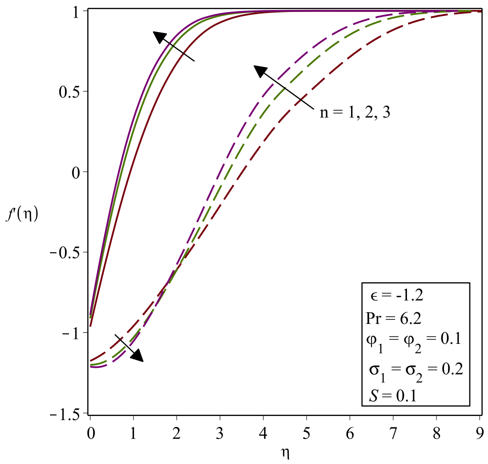

Figure 9. Velocity profile with σ_1, σ_2 and S for different n.

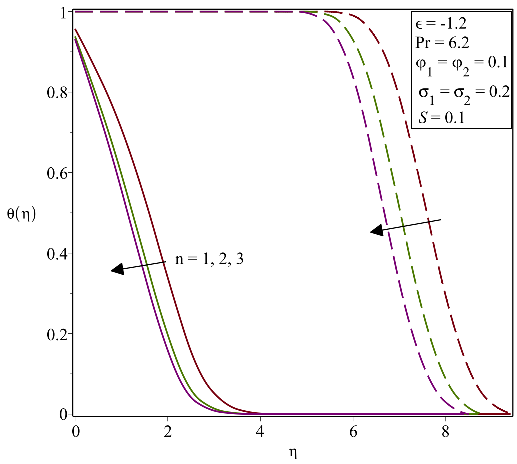

Figure 10. Temperature profile with σ_1, σ_2 and S for different n.

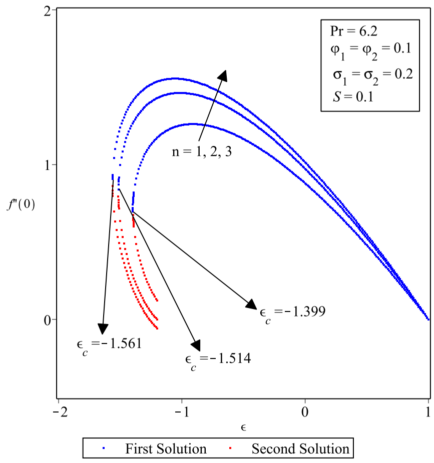

Figure 11. $f''(0)$ with ε, σ_1, σ_2 and S for different n.

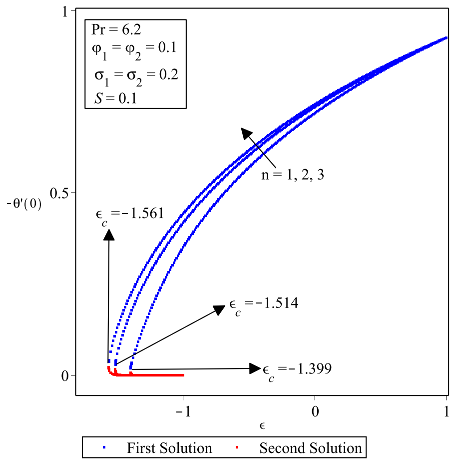

Figure 12. $-\theta'(0)$ with ε, σ_1, σ_2 and S for different n.

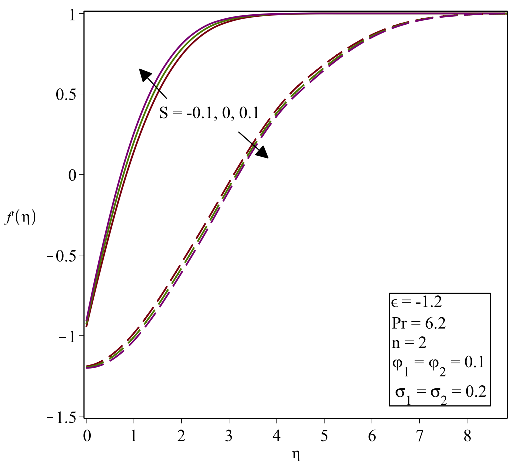

Figure 13. Velocity profile with σ_1 and σ_2 for different S.

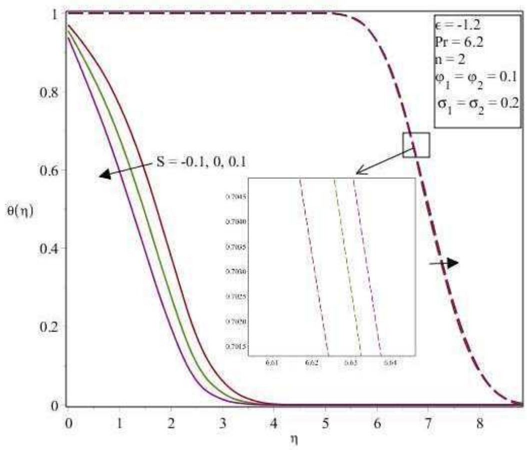

Figure 14. Temperature profile with σ_1 and σ_2 for different S.

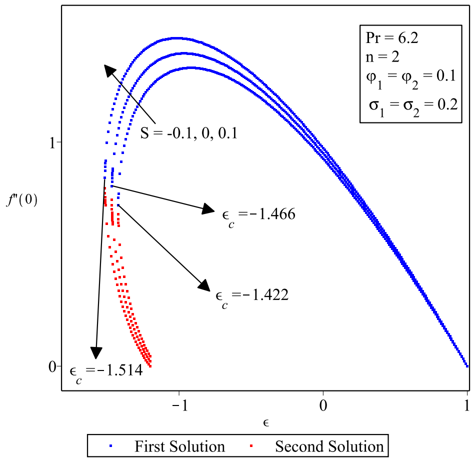

Figure 15. $f''(0)$ with ε, σ_1 and σ_2 for different S.

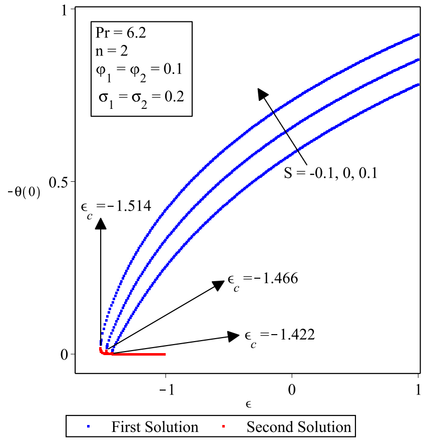

Figure 16. $-\theta'(0)$ with ε, σ_1 and σ_2 for different S.

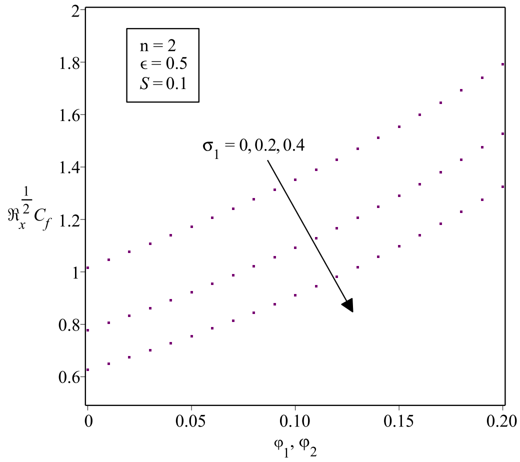

Figure 17. Local skin friction coefficient with ε and S for different σ_1.

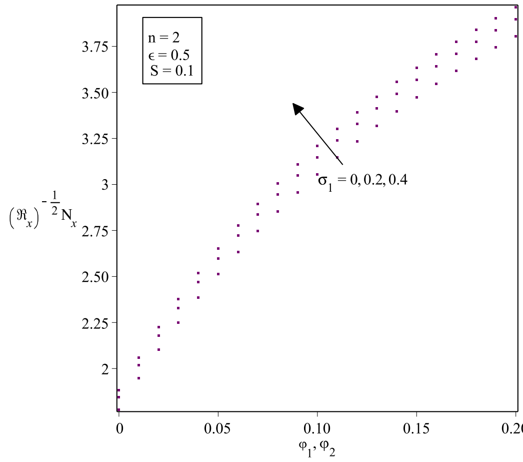

Figure 18. Local Nusselt number with ε and S for different σ_1.

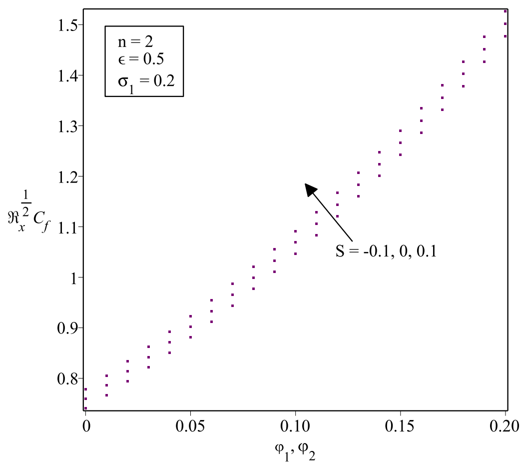

Figure 19. Local skin friction coefficient with ε and σ_1 for different S.

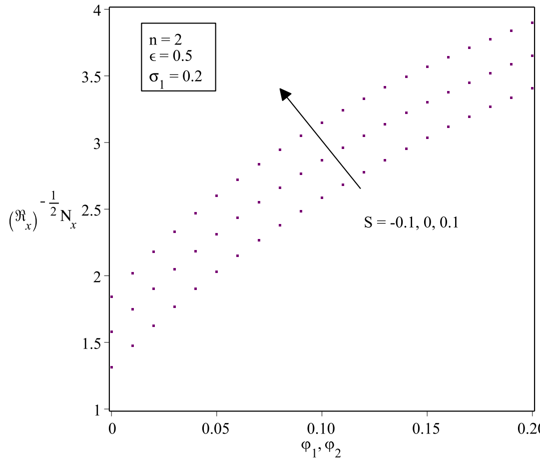

Figure 20. Local Nusselt number with ε and σ_1 for different S.

and $-\theta'(0)$ for certain values of ε and various values of the velocity slip parameter σ_1 for the hybrid nanoparticle volume fraction SWCNT and MWCNT with $\varphi_1 = \varphi_2 = 0.1$, $\sigma_2 = 0.2$, $n = 2$, and $S = 0.1$. Both graphs show the range of ε for $(\varepsilon \geqslant \varepsilon_c)$ indicate the existence of dual solutions when the value of σ_1 is increased at the boundary. For both figures, as σ_1 increases, the range of similarity solutions also increases. The same conclusion is made for the existence of duality in both figures and there is no solution whenever the values of $\varepsilon < \varepsilon_c$. This shows that the larger value of σ_1 delays the separation of boundary layers. The second solution has a lesser magnitude of $f''(0)$ and $-\theta'(0)$ as given ε rather than first solution.

Figures 9 and 10 demonstrate the outcome of different nonlinear n on the dimensionless velocity $f'(\eta)$ and temperature $\theta(\eta)$ for shrinking case which is $\varepsilon = -1.2$ using $\varphi_1 = \varphi_2 = 0.1$ with $\sigma_1 = \sigma_2 = 0.2$ and $S = 0.1$. Dual solutions are obtained in both velocity and temperature profiles. From Figure 9, it is noted that as n grows, $f'(\eta)$ rises in the momentum boundary layer for first and second solutions. Nevertheless, $\theta(\eta)$ reduces in the thermal boundary layer for both solutions as n increases. Figures 11 and 12 demonstrate the results of different values of nonlinear parameter on $f''(0)$ and $-\theta'(0)$ for certain values of ε when $\varphi_1 = \varphi_2 = 0.1$ with the presence of $\sigma_1 = \sigma_2 = 0.2$ and $S = 0.1$. For both figures, as n increases, the range of similarity solutions increases. The same conclusion is made for the existence of duality in both figures and there is no solution whenever the values of $\varepsilon < \varepsilon_c$. This indicates that the larger value of n delays the separation of the boundary layer. The second solution has a lesser magnitude of $f''(0)$ and $-\theta'(0)$ as provided ε rather than the first solution. Thus, $f''(0)$ and $-\theta'(0)$ increases due to the growing of nonlinear parameter n.

Figures 13 and 14 portray the response of different suction S values on the velocity profile $f'(\eta)$ and temperature profile $\theta(\eta)$ for shrinking case $(\varepsilon < -1)$ with $\varphi_1 = \varphi_2 = 0.1$, $\sigma_1 = \sigma_2 = 0.2$, $\varepsilon = -1.2$, and $n = 2$. From both figures, $f'(\eta)$ increases in the momentum boundary layer for first solution but decreases for second solution. But contrary result for $\theta(\eta)$ where it decreases in thermal boundary layer for first solution and it increases for second solution. Figures 15 and 16 illustrate the results of different values of suction parameter on $f''(0)$ and $-\theta'(0)$ for certain values of ε when $\varphi_1 = \varphi_2 = 0.1$ with the presence of $\sigma_1 = \sigma_2 = 0.2$ and $n = 2$. For both figures, as S increases, the range of similarity solutions also increases. The same conclusion is made for the existence of duality in both figures and there is no solution whenever the values of $\varepsilon < \varepsilon_c$. This indicates that the larger value of S delays the separation of the boundary layer. The second solution has a lesser magnitude of $f''(0)$ and $-\theta'(0)$ as provided ε rather than the first solution. Thus, $f''(0)$ and $-\theta'(0)$ increases due to the increment of suction parameter S.

Figures 17 and 18 illustrate the variations of $\mathrm{Re}_x^{\frac{1}{2}} C_f$ and $(\mathrm{Re}_x)^{-\frac{1}{2}}\mathrm{Nu}_x$ which are local skin friction coefficient and local Nusselt number respectively for various values of nanoparticle volume fraction SWCNT φ_1 and MWCNT φ_2 with different σ_1 for $\varepsilon = 0.5$, $n = 2$, and $S = 0.1$. It is noticed that the skin friction coefficient decreases when the value of σ_1 increases. Unlike local Nusselt, it increases as the value of σ_1 increases. Figures 19 and 20 show the values of $\mathrm{Re}_x^{\frac{1}{2}} C_f$ and $(\mathrm{Re}_x)^{-\frac{1}{2}}\mathrm{Nu}_x$ with different S for $\varepsilon = 0.5$, $n = 2$, and $\sigma_1 = 0.2$. It can be found that by making use of various values of hybrid nanoparticle volume fractions (φ_1, φ_2) impact a change in local skin friction and local Nusselt. As the value of S increases, the value for both $\mathrm{Re}_x^{\frac{1}{2}} C_f$ and $(\mathrm{Re}_x)^{-\frac{1}{2}}\mathrm{Nu}_x$ increase as well. Thus, it is noticed that both skin friction coefficient and local Nusselt increase when the value of S increases.

5. Conclusion

The problem of stagnation point flow over a nonlinearly stretching/shrinking sheet in hybrid carbon nanotubes with slip and suction effects was studied numerically. The consideration of the parameters such as hybrid nanoparticle volume fractions φ_1, φ_2, non-linear parameter n, velocity slip parameters σ_1, σ_2, suction parameter S, and stretching/shrinking parameter ε were solved using numerical technique based on Haar wavelets collocation.

— A unique solution exists when $\varepsilon > -1$, meanwhile dual solutions exist when $\varepsilon_c < \varepsilon \leqslant -1$ and no solution can be found where $\varepsilon < \varepsilon_c$, where ε_c is the critical value. It can be found where shrinking sheet gives dual solutions at a certain limit and stretching sheet gives unique solutions.
— The increasing of the velocity slip parameter σ_1, nonlinear parameter n, and suction parameter S postpone the boundary layer separation as both parameters widen the range of solutions.
— As nanoparticle volume fraction MWCNT φ_2 and n increase in shrinking case, both increase the velocity profile, but decrease the temperature profile for both solutions.
— When the suction parameter S increases, it increases the velocity profile for the first solution and decreases for the second solution. It also decreases the temperature profile for the first solution but increases for the second solution.
— When the velocity slip parameter σ_1 increases, it increases the velocity profile for the first solution and decreases for the second solution. But it decreases the temperature profile for both solutions.
— Local skin friction coefficient and local Nusselt number can be intensified by the increasing of nonlinear parameter n, suction S and nanoparticle volume fraction SWCNT φ_1 and MWCNT φ_2. Different result are obtained when σ_1 and nanoparticle volume fraction φ_1, φ_2 increases, local Nusselt number increases but local skin friction decreases.

Acknowledgment

This work was supported by Research Grant Putra, University Putra Malaysia.

[1] Deville M. O. An Introduction to the Mechanics of Incompressible Fluids. Springer Nature (2022).

[2] Natsiavas S., Paraskevopoulos E. A boundary layer approach to multibody systems involving single frictional impacts. Journal of Computational and Nonlinear Dynamics. American Society of Mechanical Engineers. **14** (1), 011002 (2019).

[3] Iijima S., Ichihashi T. Single-shell carbon nanotubes of 1-nm diameter. Nature. **363** (6430), 603–605 (1993).

[4] Bethune D. S., Kiang C. H., De Vries M. S., Gorman G., Savoy R., Vazquez J., Beyers R. Cobalt-catalysed growth of carbon nanotubes with single-atomic-layer walls. Nature. **363** (6430), 605–607 (1993).

[5] Navrotskaya A. G., Aleksandrova D. D., Krivoshapkina E. F., Sillanpää M., Krivoshapkin P. V. Hybrid materials based on carbon nanotubes and nanofibers for environmental applications. Frontiers in Chemistry. **8**, 546 (2020).

[6] Al-Hanaya A. M., Sajid F., Abbas N., Nadeem S. Effect of SWCNT and MWCNT on the flow of micropolar hybrid nanofluid over a curved stretching surface with induced magnetic field. Scientific Reports. **10** (1), 8488 (2020).

[7] Aladdin N. A. L., Bachok N. Duality solutions in hydromagnetic flow of SWCNT-MWCNT/water hybrid nanofluid over vertical moving slender needle. Mathematics. **9** (22), 2927 (2021).

[8] Kumar T. P., Sulochana C. Heat transfer of SWCNT-MWCNT based hybrid nanofluid boundary layer flow with modified thermal conductivity model. Journal of Advanced Research in Fluid Mechanics and Thermal Sciences. **92** (2), 13–24 (2022).

[9] Tabassum R., Al-Zubaidi A., Rana S., Mehmood R., Saleem S. Slanting transport of hybrid (MWCNTs-SWCNTs/H_2O) nanofluid upon a Riga plate with temperature dependent viscosity and thermal jump condition. International Communications in Heat and Mass Transfer. **135**, 106165 (2022).

[10] Norzawary N. H. A., Bachok N. Slip Flow Via Nonlinearly Stretching/Shrinking Sheet in A Carbon Nanotubes. Journal of Advanced Research in Micro and Nano Engineering. **14** (1), 8–19 (2023).

[11] Ahsan M., Khan A. A., Dinibutun S., Ahmad H., Jarasthitikulchai N., Sudsutad W. The Haar wavelets based numerical solution of Reccati equation with integral boundary condition. Thermal Science. **27** (Spec. issue 1), 93–100 (2023).

[12] Ahsan M., Shams-ul Haq K., Liu X., Ahmad Lone S., Nisar M. A Haar wavelets based approximation for nonlinear inverse problems influenced by unknown heat source. Mathematical Methods in the Applied Sciences. **46** (2), 2475–2487 (2023).

[13] Šarler B., Siraj-ul-Islam, Aziz I., Fazal-i-Haq. Haar wavelet collocation method for the numerical solution of boundary layer fluid flow problems. International Journal of Thermal Sciences. **50** (5), 686–697 (2011).

[14] Lepik Ü. Numerical solution of differential equations using Haar wavelets. Mathematics and Computers in Simulation. **68** (2), 127–143 (2005).

[15] Samat N. A. A., Bachok A., Arifin N. M. Boundary Layer Stagnation Point Flow and Heat Transfer over a Nonlinear Stretching/Shrinking Sheet in Hybrid Carbon Nanotubes: Numerical Analysis and Response Surface Methodology under the Influence of Magnetohydrodynamics. Computation. **12** (3), 46 (2024).

Метод колокації вейвлетів Хаара для розв'язання задачі про течію в точці гальмування над нелінійно розтяжною/стисливою поверхнею в гібридних вуглецевих нанотрубках з ефектами ковзання та всмоктування

Ханані Л.[1], Раседі А. Ф. Н.[2], Ку Л. Ф.[3], Хасваніза Н.[1], Хасан М.[4]

[1] *Кафедра математики та статистики, факультет природничих наук, Університет Путра Малайзія, 43400 Серданг, Селангор, Малайзія*

[2] *Факультет економіки та муамалату, Університет ісламських наук Малайзії, Малайзія*

[3] *Факультет гуманітарних наук, менеджменту та природничих наук, Університет Путра Малайзія, Кампус Бінтулу, 97008 Бінтулу, Саравак, Малайзія*

[4] *Центр базової підготовки до вивчення природничих наук, Університет Путра Малайзія*

Це дослідження спрямоване на вивчення течії в точці гальмування над нелінійно розтяжною/стисливою поверхнею за наявності ефектів ковзання та всмоктування у гібридних вуглецевих нанотрубках. Отримано математичну модель задачі про течію в пригничному шарі, яку розв'язано за допомогою чисельних методів на основі колокації вейвлетів Хаара. Як типи гібридних вуглецевих нанотрубок використовувалися одностінні та багатостінні нанотрубки з водою як базовою рідиною. Рівняння в частинних похідних перетворено на нелінійні звичайні диференціальні рівняння за допомогою перетворень подібності. Для роботи з цими рівняннями використано програмне забезпечення Maple. Результати представлено у вигляді графіків, що включають профілі швидкості та температури, локальний коефіцієнт поверхневого тертя та локальне число Нуссельта для різних значень концентрації гібридних наночастинок вуглецевих нанотрубок, параметра ковзання швидкості, нелінійного параметра та всмоктування. Отримані результати свідчать про те, що для поверхні, яка стискається, існують подвійні розв'язки в певних межах, тоді як для поверхні, що розтягується, розв'язки є єдиними. Крім того, параметр ефекту ковзання спричинив зменшення товщини пригничного шару та підвищення інтенсивності теплообміну.

Ключові слова: *вуглецеві нанотрубки; нелінійне розтягування/стискання; точка гальмування; вейвлет Хаара.*